ADVANCED MATERIALS
www.advmat.de

Cephalopod-Inspired Chemical-Gated Hydrogel Actuation Systems for Information 3D-Encoding Display

Baoyi Wu, Muqing Si, Luqin Hua, Dong Zhang, Wanning Li, Chuanzhuang Zhao, Wei Lu,* and Tao Chen**

Cephalopods evolve the acetylcholine-gated actuation control function of their skin muscles, which enables their dynamic/static multimode display capacities for achieving perfectly spatial control over the colors/patterns on every inch of skin. Reproduction of artificial analogs that exhibit similar multimodal display is essential to reach advanced information three-dimensional (3D) encoding with higher security than the classic 2D-encoding strategy, but remains underdeveloped. The core difficulty is how to replicate such chemical-gated actuation control function into artificial soft actuating systems. Herein, this work proposes to develop azobenzene-functionalized poly(acrylamide) (PAAm) hydrogel systems, whose upper critical solution temperature (UCST) type actuation responsiveness can be intelligently programmed or even gated by the addition of hydrophilic α-cyclodextrin (α-CD) molecules for reversible association with pendant azobenzene moieties via supramolecular host–guest interactions. By employing such α-CD-gated hydrogel actuator as an analogue of cephalopods' skin muscle, biomimetic mechanically modulated multicolor fluorescent display systems are designed, which demonstrate a conceptually new α-CD-gated "thermal stimulation-hydrogel actuation-fluorescence output" display mechanism. Consequently, high-security 3D-encoding information carriers with an unprecedented combination of single-input multiple-output, dynamic/static dual-mode and spatially controlled display capacities are achieved. This bioinspired strategy brings functional-integrated features for artificial display systems and opens previously unidentified avenues for information security.

1. Introduction

Stimuli-responsiveness is essential for the living of natural organisms.[1] To ensure perfect adaptation to the changing environment, stimuli-responsiveness of many important biological processes has evolved to be capable of being intelligently programmed or even gated.[2] One famous example is the environment-adaptive color change of cephalopods' skin.[3] Anatomical studies have revealed that there exist several types of chromatophores ringed by radial muscles in the cephalopods' skin.[4] The skin colors/patterns are then regulated by bioelectricity-responsive releasing/contracting actuation of these radial muscles, which instantly induces mechanical expansion/contraction of corresponding chromatophores and manifests as skin color/pattern changes. Nevertheless, to better match different environment background colors, neurotransmitter inhibitor such as acetylcholine may be secreted under some circumstances to reset membrane potential for precisely deactivating the actuation responsiveness of certain radial muscles (**Scheme 1a**).[5] When the secreted acetylcholine molecules are metabolized over time, such acetylcholine-gated muscle

B. Wu, M. Si, W. Li, W. Lu, T. Chen
Laboratory of Advanced Marine Materials
Ningbo Institute of Materials Technology and Engineering
Chinese Academy of Sciences
Ningbo 315201, China
E-mail: luwei@nimte.ac.cn

B. Wu, M. Si, W. Li, W. Lu, T. Chen
School of Chemical Sciences
University of Chinese Academy of Sciences
19A Yuquan Road, Beijing 100049, China
E-mail: tao.chen@nimte.ac.cn

L. Hua, C. Zhao
School of Materials Science & Chemical Engineering
Ningbo University
Ningbo 315211, China
E-mail: zhaochuanzhuang@nbu.edu.cn

D. Zhang
The Wallace H. Coulter Department of Biomedical Engineering
Georgia Institute of Technology and Emory University
Atlanta, GA 30332, USA

T. Chen
College of Material Chemistry and Chemical Engineering
Key Laboratory of Organosilicon Chemistry and Material Technology
Ministry of Education
Hangzhou Normal University
Hangzhou 311121, China

The ORCID identification number(s) for the author(s) of this article can be found under https://doi.org/10.1002/adma.202401659

DOI: 10.1002/adma.202401659

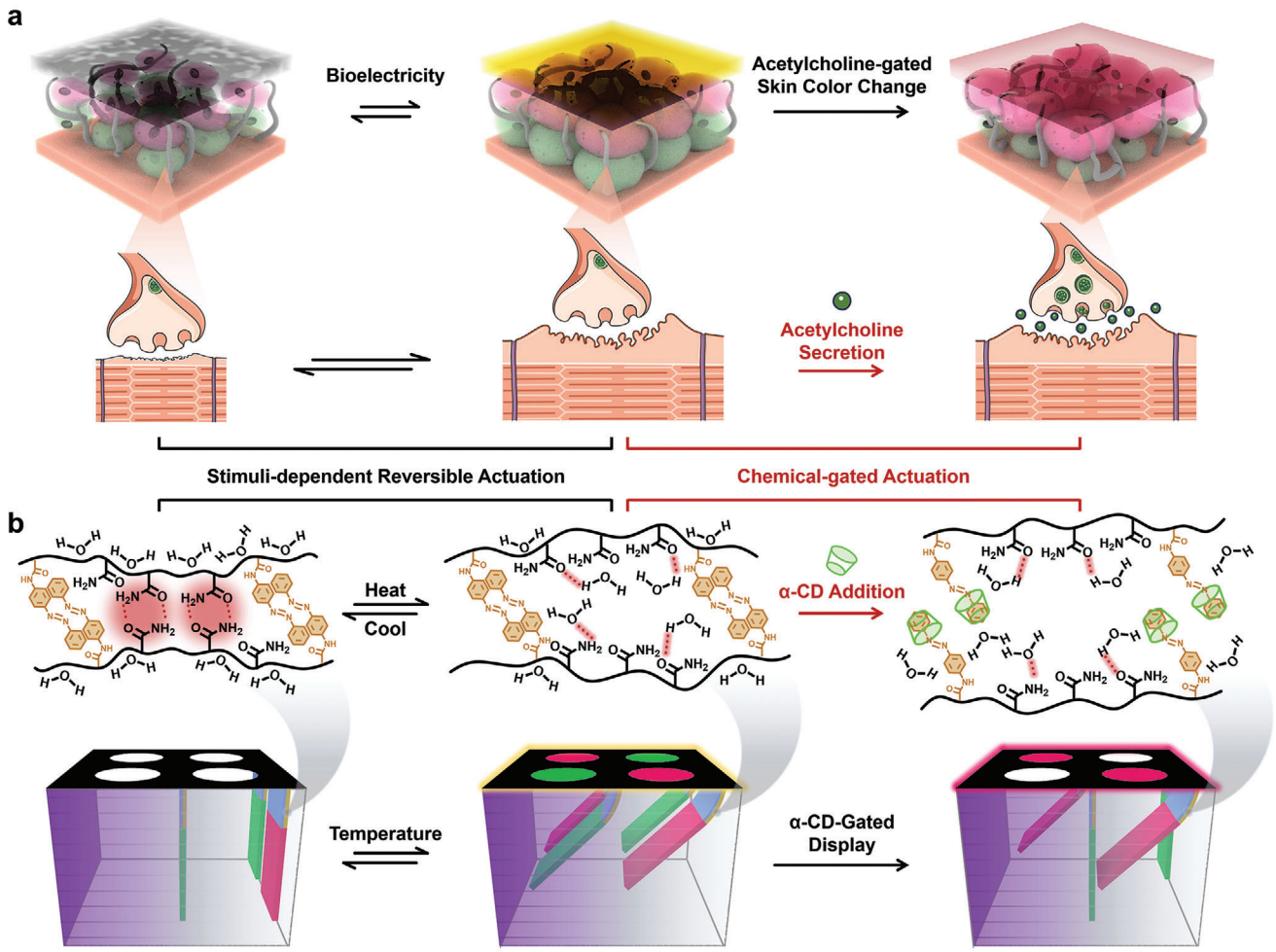

Scheme 1. Illustration of the biomimetic basis to replicate natural chemical-gated actuation control capacity of cephalopods' skin muscles to produce chemical-gated hydrogel actuation systems for information three-dimensional (3D) encoding display. a) Illustration showing the acetylcholine-gated actuation control capacity of cephalopods' skin muscles for perfect skin color/pattern display. The cephalopods' skin muscles usually generate reversible expansion under bioelectrical stimulation. Nevertheless, to better match different environment background colors, neurotransmitter inhibitor such as acetylcholine may be secreted under some circumstances to reset membrane potential for precisely deactivating the actuation responsiveness of certain radial muscles. b) Illustration showing the chemical design of artificial α-cyclodextrin (α-CD) gated hydrogel actuation systems for information 3D-encoding display. The hydrophobic azobenzene-functionalized hydrogel exhibits upper critical solution temperature (UCST) type thermoresponsive actuating behavior. Nevertheless, its actuation responsiveness can be completely deactivated by the addition of hydrophilic α-CD molecules for association with the pendant azobenzene groups via host–guest interactions, just like that of cephalopods' skin muscles in the presence of acetylcholine.

actuation responsiveness will be spontaneously recovered. It is through such chemical-gated muscle actuation control function that cephalopods have the dynamic/static multimode display capacity to achieve perfectly spatial control over the colors/patterns on every inch of skin, which is essential for information delivery (e.g., warning, camouflaging) to their co-existing organisms in dynamic living environment.

Cephalopods' skin has been a source of inspiration in the development of intelligent luminescence-color changeable display systems that are designed to emulate the wonderful function of their biological counterparts for diverse applications such as dynamic camouflage, stretchable electronics, and especially information encryption.[6] In the context, the past decade has witnessed a large number of luminescent display systems, in which dynamic information encoding/decoding is achieved by utilizing stimuli-responsive reversible covalent molecular or noncovalent aggregation structure changes of the incorporated fluorophores.[7] Nevertheless, this classic strategy is usually limited to producing stimuli-dependent dynamic information display, but fails to achieve the stimuli-independent static information display.[8] Such capacity is thus far inferior to that of cephalopods' skin which allows for intelligent switch between dynamic/static dual-mode display via the acetylcholine-gated muscle actuation control. Additionally, most reported examples, despite state-of-the-art, primarily coded data in single 2D planes.[9] As such, the written luminescent information may be easily decrypted, for instance, under the irradiation of one ultraviolet light.[10] Therefore, they generally underutilized the possibility to learn about the delicate three-dimensional (3D) structure of cephalopods' skin, which consists of the out-layer skin as

displayer and underlying radial muscles as modulator, for achieving information 3D-encoding with enhanced display security. With these discussions in mind, we begin to speculate that, if such natural chemical-gated actuation capacity was replicated, it would produce truly biomimetic actuators that could behave like cephalopods' skin muscles to intelligently gate their actuation responsiveness. More importantly, such chemical-gated actuators might be further explored to design robust types of mechanically modulated 3D display systems, which not only enabled the stimuli-responsive dynamic information display, but also could be selectively gated to achieve stimuli-independent static information display. Such dynamic/static dual-mode display and high-security 3D-encoding capabilities are highly expected to meet the differential display requirements for various kinds of information, but has not been demonstrated.

The key difficulty for such demonstration is to replicate the chemical-gated actuation control function of cephalopods' skin muscles into artificial soft actuating systems. To do this, soft actuators such as polymeric hydrogel with muscle-like soft wet nature and molecule permeability is chosen as the proof-of-concept material in this study.[11] As illustrated in Scheme 1b, the hydrogel was designed by radical copolymerization of the hydrophobic azobenzene-containing acrylamide (ABAM) monomer with commercial acrylamide (AAm) monomer in order to decrease the ΔS of the hydrophilic PAAm chain segments.[12] Consequently, zipper-like multiple H-bonds could be generated to induce upper critical solution temperature (UCST) type thermoresponsive actuating behavior of the hydrogels that were capable of swelling in the higher temperature while shrinking in the lower temperature. Astonishingly, such thermoresponsive actuating behavior was found to be continuously programmed or even completely deactivated by the addition of α-CD molecules. This was because hydrophilic α-CD was able to spontaneously bind the pendant azobenzene groups via host–guest interactions and thus gradually vary thermal-responsiveness of the hydrogels. When all the pendant azobenzene groups were captured by α-CD, the hydrogels' actuation responsiveness would be completely erased, just like that of cephalopods' skin muscles in the presence of acetylcholine. On the basis of this bioinspired hydrogel system with intelligent α-CD-gated actuation responsiveness, multicolor fluorescent hydrogel actuators were designed. Furthermore, by utilizing the α-CD-gated multicolor fluorescent hydrogel actuators as analogues of cephalopods' skin muscles, biomimetic mechanically modulated display systems were designed, which demonstrated a chemical-gated "thermal stimulation-hydrogel actuation-fluorescence output" display mechanism. As a consequence, high-security 3D-encoding information carriers with an unprecedented combination of single-input multiple-output, dynamic/static dual-mode and spatially controlled display capacities were finally constructed for intelligent information encryption with enhanced security.

2. Result and Discussion

2.1. Chemical Design and Molecular Mechanism of UCST-Type Thermoresponsive P(AAm-*co*-ABAM) Hydrogel

In the conventional design principles of thermoresponsive polymers, poly(acrylamide) (PAAm) has usually been identified as a nonthermoresponsive polymer in water media.[12] Interestingly, by copolymerizing the hydrophilic AAm with hydrophobic monomers to enhance the interchain hydrophobic aggregation, amide-amide H-bonds are expected be generated in the obtained polymer chains between the amino group (H-donor) and the carbonyl group (H-acceptor). The amide-amide H-bonds can be broken with external thermal energy, so the nonthermoresponsive PAAm polymer can be converted into a UCST-type thermoresponsive copolymer.[12] Based on this thermodynamic theory, we designed a hydrophobic monomer, ABAM (Figure S1, Supporting Information), and subsequently synthesized the P(AAm-*co*-ABAM) hydrogel through copolymerization of ABAM with AAm in DMSO and dialysis in water. As expected, upon transferring the P(AAm-*co*-ABAM) hydrogel from 60 °C water to 0 °C water, it quickly became opaque (**Figure 1a**). This phenomenon indicated that the P(AAm-*co*-ABAM) chains underwent a thermoresponsive phase transition, and the collapse of the polymer chains caused the hydrogel to lose transparency. According to the experiment results, together with the assistance of finite simulations, the molecular mechanism behind the aforementioned UCST thermoresponsiveness was elucidated and illustrated. Since the grafted amide groups of ordinary PAAm chains were very hydrophilic and thus preferred to form H-bonds with water molecules. It was the significant increase in entropy (ΔS) associated with this hydrophilic interaction between grafted amide groups and water molecules that typically derived PAAm hydrogels to favor dissolution in water, resulting in the absence of thermoresponsiveness (Figure 1b). In contrast, through copolymerization with azobenzene monomers, the polymer chain segments would be forced to become associated by the hydrophobic aggregation of azobenzene moieties, which diminished the ΔS, repelling water molecules to facilitate the formation of zipper-like amide-amide H-bonds. Consequently, the P(AAm-*co*-ABAM) hydrogels were endowed with UCST responsiveness (Figure 1c).

To confirm the mechanism discussed above, the Raman spectra of the P(AAm-*co*-ABAM) hydrogel were measured at 4 °C and 80 °C, respectively. As depicted in Figure 1d, the entire spectrum of azobenzene group shifted toward the lower wavenumbers at lower temperatures, especially the C—N stretching peak that clearly shifted from 1145 to 1136 cm^{-1} as the temperature decreased from 80 °C to 4 °C.[13] Similar results were also observed in their temperature-dependent FT-IR spectra. As shown in Figure S2 (Supporting Information), the characteristic peak at 3250 cm^{-1} was gradually intensified upon environmental temperature decrease, which indicated the enhanced intramolecular hydrogen bonds of the hydrogel at low temperature.

Moreover, urea, a molecule containing both H-donors and H-acceptors, was introduced into the P(AAm-*co*-ABAM) network at low temperatures. Due to the competitive effect, urea would break the existing zipper-like H-bonds by forming hydrogen bond interactions with single P(AAm-*co*-ABAM) chains (Figure S3a, Supporting Information). As demonstrated in Figure S3b (Supporting Information), as the urea concentration increased from 0 to 2 M, the characteristic peak at 1136 cm^{-1} gradually shifted to 1143 cm^{-1}. This process was similar to the situation observed when transferring the P(AAm-*co*-ABAM) hydrogel from 4 °C to 80 °C. These facts support the notion that the generation of zipper-like multi-H-bonds restricts the stretching vibrational mode of the azobenzene group and leads to the shift in the

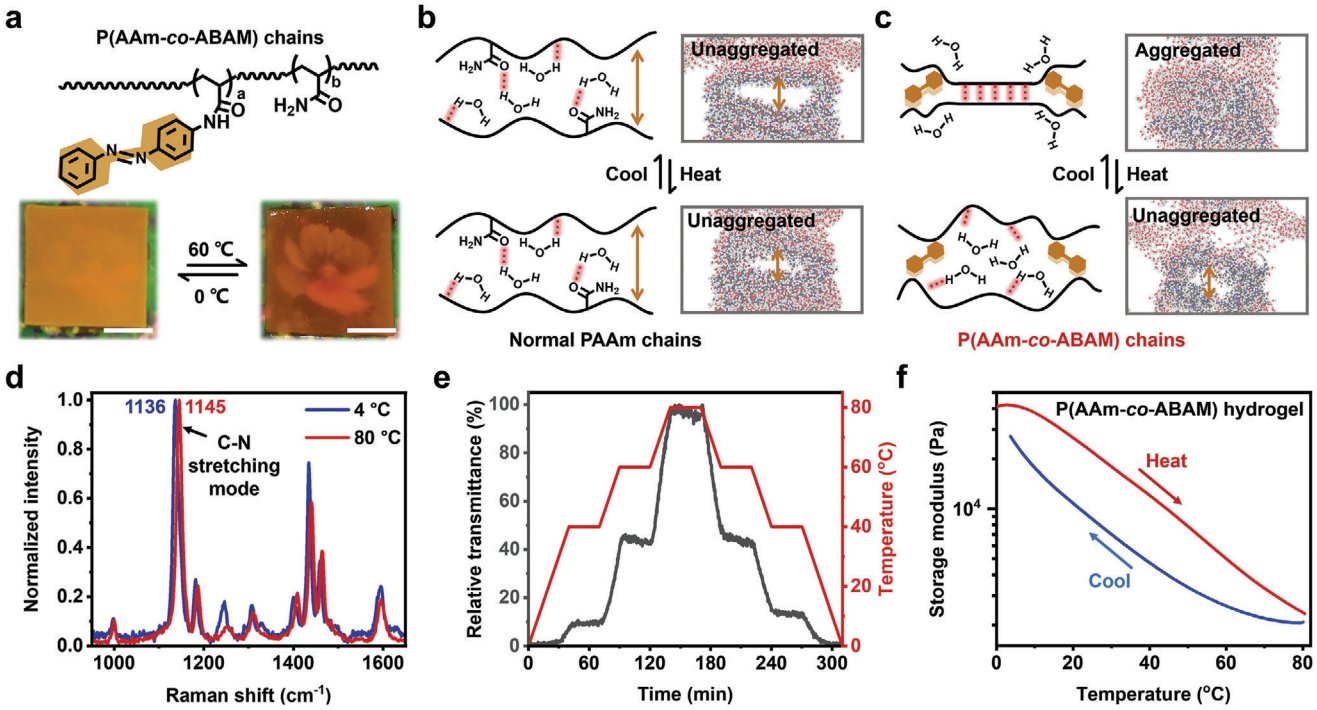

Figure 1. Upper critical solution temperature (UCST) type thermoresponsiveness of P(AAm-*co*-ABAM) hydrogel. a) Chemical structure of P(AAm-*co*-ABAM) hydrogel and the photo showing its transmittance change at 0 °C and 60 °C. b-c) Illustration and finite simulation showing the molecular mechanism of normal PAAm chains and P(AAm-*co*-ABAM) chains during reversible heating and cooling process. d) Raman spectra of P(AAm-*co*-ABAM) hydrogel recorded at 4 °C and 80 °C, respectively. e) Relative transmittance curve of P(AAm-*co*-ABAM) hydrogel with stepwise temperature variation. f) Storage modulus change of P(AAm-*co*-ABAM) hydrogel during reversible heating and cooling process. Scale bars: 1 cm.

Raman spectrum. Furthermore, the FT-IR spectra of the P(AAm-*co*-ABAM) hydrogel were evaluated and provided further proof of the existence of intermolecular hydrogen bonds (Figure S4, Supporting Information). Additionally, to elucidate the role of chain hydrophobicity in this phase transition process, we conducted a contact angle test to assess the hydrophobic effect of the azobenzene group. As shown in Figure S5 (Supporting Information), despite the gradual breaking of internal H-bonds with increasing urea concentration, the contact angle of the P(AAm-*co*-ABAM) hydrogel remained stable. This observation suggested that the UCST-type phase transition process did not impact the internal hydrophobic effect. Therefore, the thermoresponsiveness of the P(AAm-*co*-ABAM) hydrogel should be attributed to the dynamic generation of the zipper-like H-bonds.

To further evaluate and quantify the degree of the UCST-type phase transition process, temperature-dependent transmittance measurement was applied. According to the result of Figure S6 (Supporting Information), P(AAm-*co*-ABAM) hydrogels exhibit two different features: one is the wide phase transition window and the other one is a thermodynamically induced stepwise phase transition, in comparison with existing thermoresponsive polymers with narrow phase transition temperatures.[14] In detail, when the P(AAm-*co*-ABAM) hydrogel was placed in a cyclical heating/cooling environment, it exhibited continuous transmittance changes from 0 °C to 80 °C, indicating a fairly wide phase transition range. It was possibly because the polydisperse distribution of azobenzene groups and cross-linkers in the chain network, which led to a polydisperse stability of the H-bonds between azobenzene.[15] Such a feature could be used to realize a stepwise transmittance change (Figure 1e). Besides, this distinctive UCST-type thermoresponsiveness could be also observed in alterations to the modulus owing to the reversible zipper-like multiple H-bonds. At low temperature, the H-bonds acted as temporary cross-linking points, increasing the modulus of the P(AAm-*co*-ABAM) hydrogel. Consequently, the hydrogel became tougher at low temperatures while softer at high temperatures. As depicted in Figure 1f, the storage modulus of the P(AAm-*co*-ABAM) hydrogel exhibited a continuous change within the cyclical heating/cooling process from 0 °C to 80 °C. This behavior confirmed the wide range of UCST-type thermoresponsiveness displayed by the P(AAm-*co*-ABAM) hydrogel.

Overviewing existing studies about thermoresponsive polymers,[16] the distinctive thermoresponsive behavior of the P(AAm-*co*-ABAM) hydrogel could be considerable in two reasons. On one hand, conventional thermoresponsive polymers are usually synthesized through living radical polymerization methods such as atom transfer radical polymerization (ATRP) and reversible addition-fragmentation chain transfer polymerization (RAFT), which endow the polymer with a narrow distribution of molecular weight.[17] In contrast, our P(AAm-*co*-ABAM) hydrogels were prepared via ordinary radical polymerization, resulting in a wider molecular weight distribution. This wider distribution contributes to the formation of multilevel H-bonds and a wider phase transition temperature range. On the other hand, the introduction of chemical cross-linking points in the hydrogel system further decreases the degree of

polymerization in the chain segments, limiting the number of polymer configurations and expanding the phase transition window. In fact, evidence showed that increasing the cross-linking degree of P(AAm-*co*-ABAM) hydrogels from 4% to 8% leads to an increase in relative transmittance from 0% to 30% at low temperatures, indicating that the actual phase transition temperature spans the range of 0 °C to 80 °C (Figure S7, Supporting Information). Similarly, corresponding rheological behavior also confirmed this observation (Figure S8, Supporting Information).

2.2. α-CD-Gated Thermoresponsiveness of P(AAm-co-ABAM) Hydrogel Via Supramolecular Host–Guest Interaction

As previously discussed, it was the hydrophobic aggregation of azobenzene groups that induced the dynamic generation of zipper-like multi-H-bonds, thereby providing the P(AAm-*co*-ABAM) hydrogel with distinctive thermoresponsiveness. Surprisingly, we observed that by simple addition of α-cyclodextrin (α-CD), the hydrophilicity, swelling characteristics, and corresponding thermoresponsiveness of the hydrogel could be mutually influenced. For instance, when the hydrophobic azobenzene group interacted with the hydrophilic α-CD via host–guest interactions, it resulted in the gradual dissociation of hydrophobic clusters within the P(AAm-*co*-ABAM) hydrogel, leading to a shift toward a more hydrophilic state. This alteration initiated the swelling process and diminished the thermoresponsiveness of the hydrogel (**Figure 2a**). To demonstrate this phenomenon, swelling experiments were conducted in this study, in which the swelling hydrogel length was denoted as L and the original length was denoted as L_0. The swelling ratio of the P(AAm-*co*-ABAM) hydrogel strips, defined as $(L - L_0)/L_0$, was thus used to evaluate the swelling situation. When 0.1 mmol α-CD was introduced into the P(AAm-*co*-ABAM) hydrogel strip in 40 mL of water, the hydrogel strip underwent significant swelling, expanding from an initial length of 20 to 30 mm as the hydrophilicity of the polymer chains gradually increased (Figure S9, Supporting Information). Moreover, the enhanced hydrophilicity of the P(AAm-*co*-ABAM) chains facilitated increased freedom of chain mobility, leading them to favor dissolution in water, resulting in weakened thermoresponsiveness. These hypotheses were further supported by transmittance and rheological behavior tests (Figures S10 and S11, Supporting Information).

Notably, thanks to the precise host–guest interactions between the grafted azobenzene groups and α-CD, the hydrophilicity of the P(AAm-*co*-ABAM) chains showed a strong dependence on the addition amount of α-CD and thus could be continuously regulated. As shown in Figure 2b, when 0.02 mmol of α-CD was added into 40 mL of water where the α-CD/ABAM molar ratio was 1:1, the hydrogel swelling ratio would increase to 0.15 after reaching swelling equilibrium. Subsequently, if additional 0.02 mmol of α-CD was added to increase the α-CD/ABAM molar ratio from 1:1 to 2:1, the hydrogel strip would further swell to enlarge the swelling ratio from 0.15 to 0.32. Interestingly, if the initial addition of α-CD was 0.04 mmol (α-CD/ABAM molar ratio was 2:1), the hydrogel strip would be heavily swollen to reach the swelling ratio of 0.30. This result paralleled the outcome achieved when α-CD was stepwisely added to attain α-CD/ABAM ratio of 2:1. Similar phenomena were observed at higher α-CD concentrations (Figure 2c). These findings indicated that the hydrophilicity of the P(AAm-*co*-ABAM) hydrogel can be precisely and continuously modulated by controlling the addition amount of α-CD.

Based on the α-CD-regulated hydrophilicity of P(AAm-*co*-ABAM) chains, thermoresponsive swelling property of the hydrogel could also be further programmed or even gated. Initially, the swelling ratio of untreated P(AAm-*co*-ABAM) hydrogel strips would increase to 0.19 within 30 min in 60 °C water (Figure 2d). Besides, it could further demonstrate a wider thermoresponsive swelling range from 0.06 to 0.28 owing to the wider phase transition temperature range of P(AAm-*co*-ABAM) network (Figure S12, Supporting Information). Additionally, the swollen hydrogel could revert to its original state when the external temperature was reduced to 0 °C, and this cyclic behavior could be repeated more than 10 times (Figure S13, Supporting Information). Furthermore, by utilizing α-CD to bind the grafted azobenzene groups via host–guest interactions, we were able to continuously regulate its thermoresponsiveness. Through evaluating the thermoresponsive swelling properties of the P(AAm-*co*-ABAM) hydrogel in aqueous solutions of α-CD (Figure S14, Supporting Information), it was observed that the thermoresponsiveness of the hydrogel gradually diminished (Figure 2e). This result demonstrated that, unlike the conventional strategy of adjusting the copolymerization ratio during the polymerization process to regulate the thermoresponsiveness, our system utilized dynamic supramolecular interaction to efficiently control the thermoresponsiveness of the P(AAm-*co*-ABAM) hydrogel after material manufacture.

It is important to note that the coordinated α-CD could also be efficiently removed by immersing the P(AAm-*co*-ABAM) hydrogel in pure water or adding a competitive guest such as adamantane to reset its thermoresponsiveness. As shown in Figure S15 (Supporting Information), when the P(AAm-*co*-ABAM) hydrogel was immersed into 5 mg mL^{-1} α-CD solution, the FT-IR signals in the range of 1800 to 950 cm^{-1}, which were assigned to H-bond interactions, were shielded owing to the host–guest interactions between the grafted azobenzene groups and α-CD. Similarly, based on the Raman evaluation, the characteristic peak of the azobenzene group in the range of 1100 to 1600 cm^{-1} was also significantly reduced, further confirming this coordination. Furthermore, after immersing the hydrogel in pure water for 24 h, these signals would reappear and recover to their original state (Figure S16, Supporting Information). These results fully demonstrated the reversibility of the aforementioned supramolecular host–guest interaction and confirm the α-CD-gated thermoresponsiveness of this hydrogel system.

2.3. α-CD-Gated Actuation Control of the Bilayer P(AAm-co-ABAM) Actuator

Although P(AAm-*co*-ABAM) hydrogels have the capability to exhibit α-CD-gated thermoresponsiveness via supramolecular host–guest interaction, their shape-morphing process is still limited due to their isotropic structure. To overcome this limitation, the interfacial diffusion polymerization (IDP) strategy was applied to grow a passive PAAm hydrogel layer on the surface of the as-prepared P(AAm-*co*-ABAM) hydrogel for enabling anisotropic deformation (**Figure 3a**).[2b] Based on the tough bilayer structure,

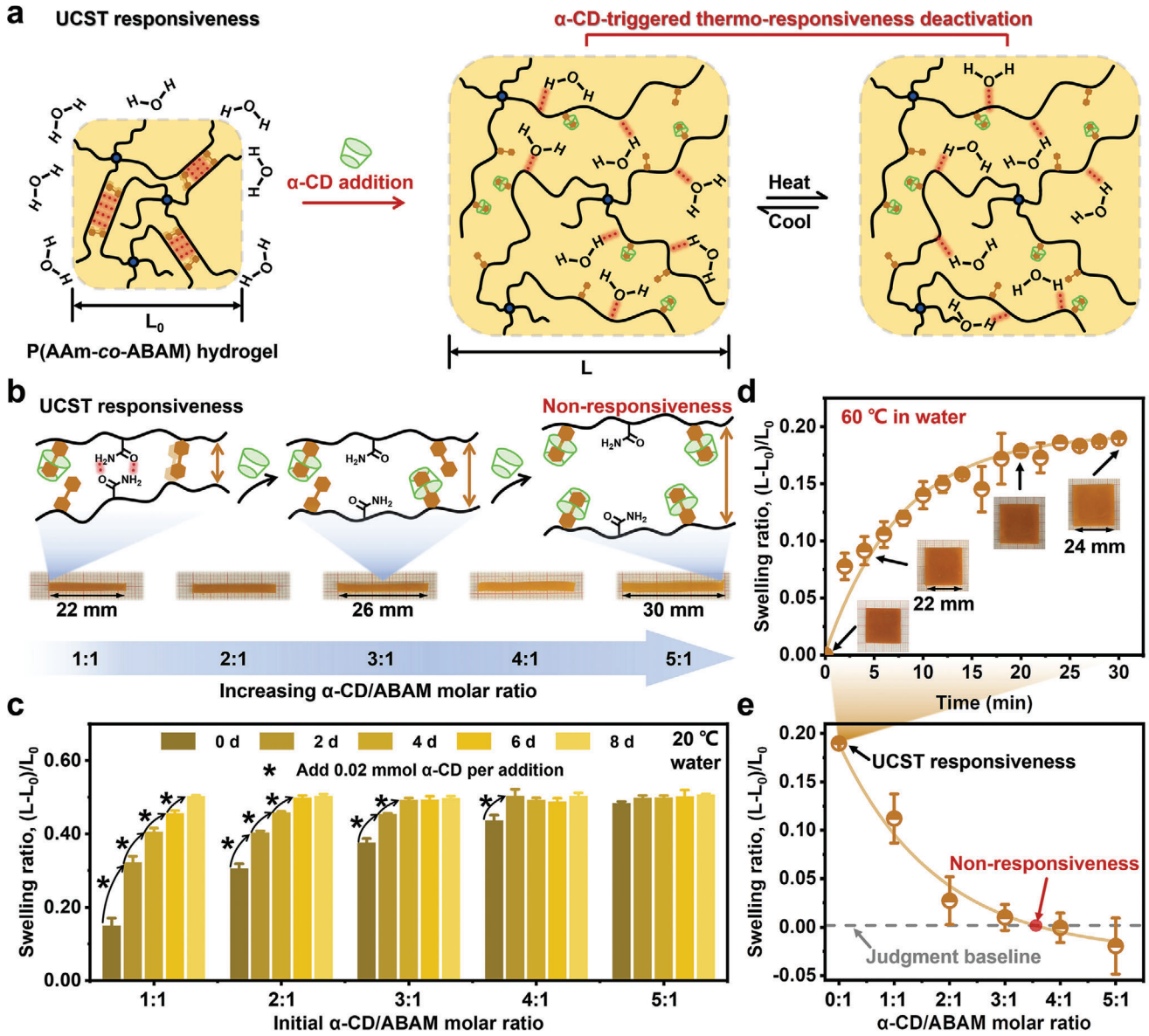

Figure 2. α-cyclodextrin (α-CD) gated thermoresponsiveness of P(AAm-*co*-ABAM) hydrogel via supramolecular host–guest interaction. a) Illustration showing the α-CD-gated thermoresponsiveness deactivation mechanism of P(AAm-*co*-ABAM) hydrogel. b) Illustration and images showing the length change of P(AAm-*co*-ABAM) hydrogel stripes after being treated in the solutions with different α-CD feed ratio. c) The swelling ratio of P(AAm-*co*-ABAM) hydrogel stripes in the solutions with different α-CD feed ratio. Hydrogel stripes were immersed in 40 mL pure water initially, and α-CD was then gradually added to reach different α-CD/ABAM molar ratio. The error bars were obtained from the swelling experiments of four independent P(AAm-*co*-ABAM) hydrogel stripes. d) Swelling ratio of original P(AAm-*co*-ABAM) hydrogel strip in 60 °C water. The error bars were obtained from the swelling experiments of four independent P(AAm-*co*-ABAM) hydrogel sheets. e) Thermo-triggered relative swelling ratio of P(AAm-*co*-ABAM) hydrogel that have been pretreated in the solutions with different α-CD/ABAM molar ratio. L and L_0 denote the length of P(AAm-*co*-ABAM) hydrogel sample measured at 60 °C and 0 °C, respectively. The error bars were obtained from the swelling experiments of four independent P(AAm-*co*-ABAM) hydrogel stripes.

when the swelling layer expanded, the deformation difference leaded to stress in the two layers. This stress caused a net moment and allowed the whole structure to bend toward the passive layer. The phenomena could be understood by finite element modeling. As can be seen from Figure S17a (Supporting Information), the simulation result is consistent with the measured Δ bending angles of P(AAm-*co*-ABAM) hydrogels. On the basis of these simulation results, the bending performance could be quantitatively linked to the degree of swelling (Figure S17b, Supporting Information), suggesting that Δ bending angles of P(AAm-*co*-ABAM) hydrogels are positively correlated to its swelling ratio. Since the property of bilayer hydrogel actuator was known to depend on its parameters such as the thicknesses, lengths, and widths, optimized experiments were thoroughly conducted (Figure S18, Supporting Information), which indicated that the hydrogel actuator with the length/width ratio of 10/1 and passive layer

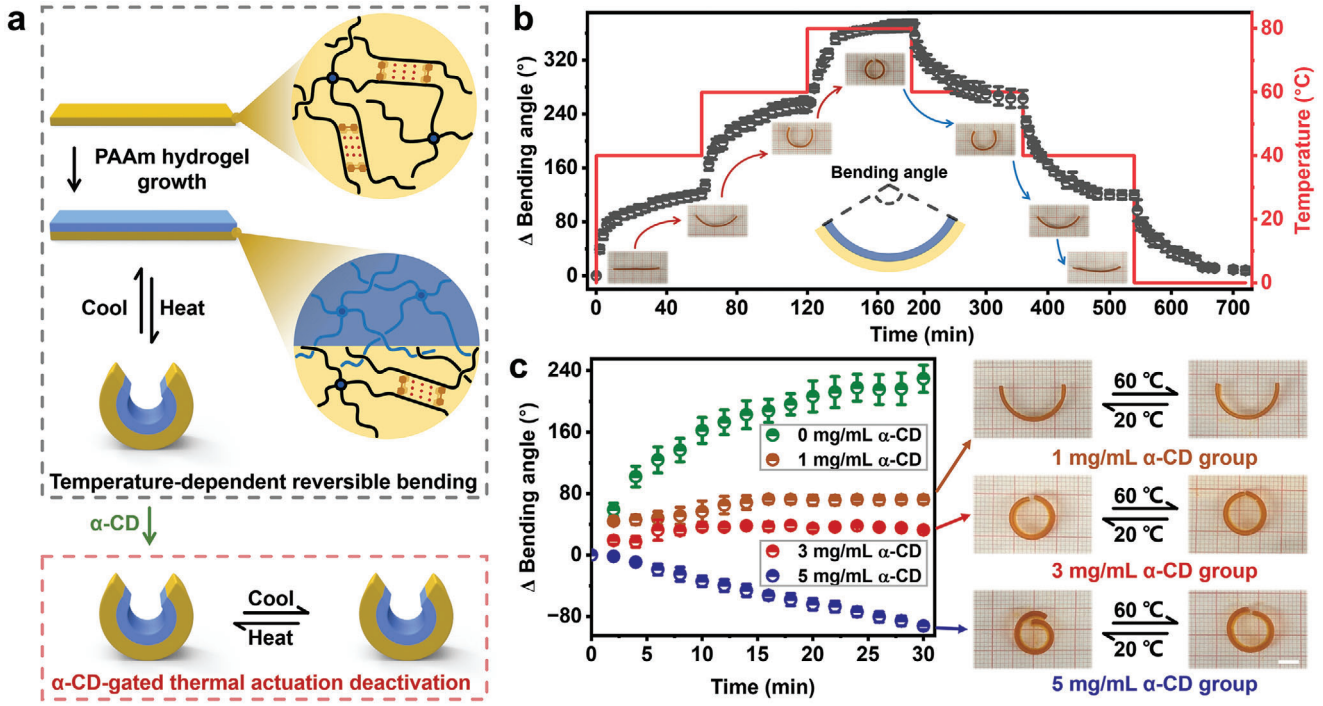

Figure 3. Fabrication of the bilayer P(AAm-*co*-ABAM) actuator and its α-cyclodextrin (α-CD) gated actuation control. a) Illustration showing the fabrication of bilayer P(AAm-*co*-ABAM) actuator and its actuation behavior. b) The temperature-dependent bending angle profile of bilayer P(AAm-*co*-ABAM) actuators recorded as a function of time. The error bars were obtained from the Δ bending angle experiments of four independent bilayer P(AAm-*co*-ABAM) actuator. c) The time-dependent Δ bending angle profile of bilayer P(AAm-*co*-ABAM) actuators in several α-CD solutions (0, 1, 3, and 5 mg mL^{-1}), as well as the corresponding photos showing their actuation results. Herein, Δ bending angle is defined as the difference between the bending angles recorded at 60 °C and 20 °C. The error bars were obtained from the Δ bending angle experiments of four independent bilayer P(AAm-*co*-ABAM) actuators. Scale bar: 0.5 cm.

thickness of 0.2 mm exhibited larger bending angles. Consequently, the obtained bilayer actuator could demonstrate reversible and cyclic bending deformation in response to external temperature changes (Figure S19, Supporting Information). Benefited from the special thermoresponsiveness of P(AAm-*co*-ABAM) hydrogels, the bending states could also be regulated by programmatically controlling the external temperatures (Figure 3b).

Similar to isotropic P(AAm-*co*-ABAM) hydrogels, the α-CD-gated thermoresponsiveness deactivation was also observed for the bilayer P(AAm-*co*-ABAM) actuator. For instance, the original P(AAm-*co*-ABAM) actuator could bend over 220° at 60 °C, but could only achieve a Δ bending angle of around 70° in the 1 mg mL^{-1} α-CD solution (Figure 3c). As discussed in this manuscript, α-CD could bond with the hydrophobic azobenzene groups of P(AAm-*co*-ABAM) hydrogel via host–guest interactions to diminish its UCST-type responsiveness. Consequently, its time-dependent Δ bending angles were kept positive at low-concentration α-CD solutions (<3 mg mL^{-1}), but gradually decreased with increasing α-CD concentration. When α-CD concentration reached 5 mg mL^{-1}, nearly all the hydrophobic azobenzene groups of P(AAm-*co*-ABAM) hydrogel had been bonded by α-CD to make the hydrogel completely hydrophilic at 20 °C. Since the host–guest interactions between α-CD and azobenzene groups are highly dynamic, part of the bonded α-CD may be dissociated at high temperature (60 °C) to decrease the hydrophilicity and water-absorbing capacity of P(AAm-*co*-ABAM) hydrogel. Therefore, negative Δ bending angle of P(AAm-*co*-ABAM) hydrogel was observed in 5 mg mL^{-1} α-CD solution.

2.4. Thermomechanical Display Via an α-CD-Gated "Thermal Stimulation-Hydrogel Actuation-Fluorescence Output" Cascading Mechanism

By mimicking the acetylcholine-gated actuating responsiveness of radial muscles around cephalopods' skin chromatophores, we have demonstrated intelligent azobenzene-functionalized hydrogel actuators whose thermal actuating responsiveness could be continuously programmed and even reversibly gated by the α-CD molecules via supramolecular host–guest interaction. This progress further encouraged us to explore their possibility for preparing artificial display systems that could behave like natural cephalopods' skin to enable on-demand multicolor display. To do this, thermomechanical fluorescent hydrogel actuator was firstly designed and prepared through series connection of the bilayer P(AAm-*co*-ABAM) hydrogel actuator and the Eu^{3+}/Tb^{3+}-coordinated multicolor fluorescent P(AAm-*co*-K6MUPA) hydrogel block (**Figure 4a**). Taking Eu^{3+}-coordinated hydrogel system shown in Figure 4b as an example, such series-connected red fluorescent hydrogel block could be actuated to bend left by the heat-triggered deformation of top P(AAm-*co*-ABAM)

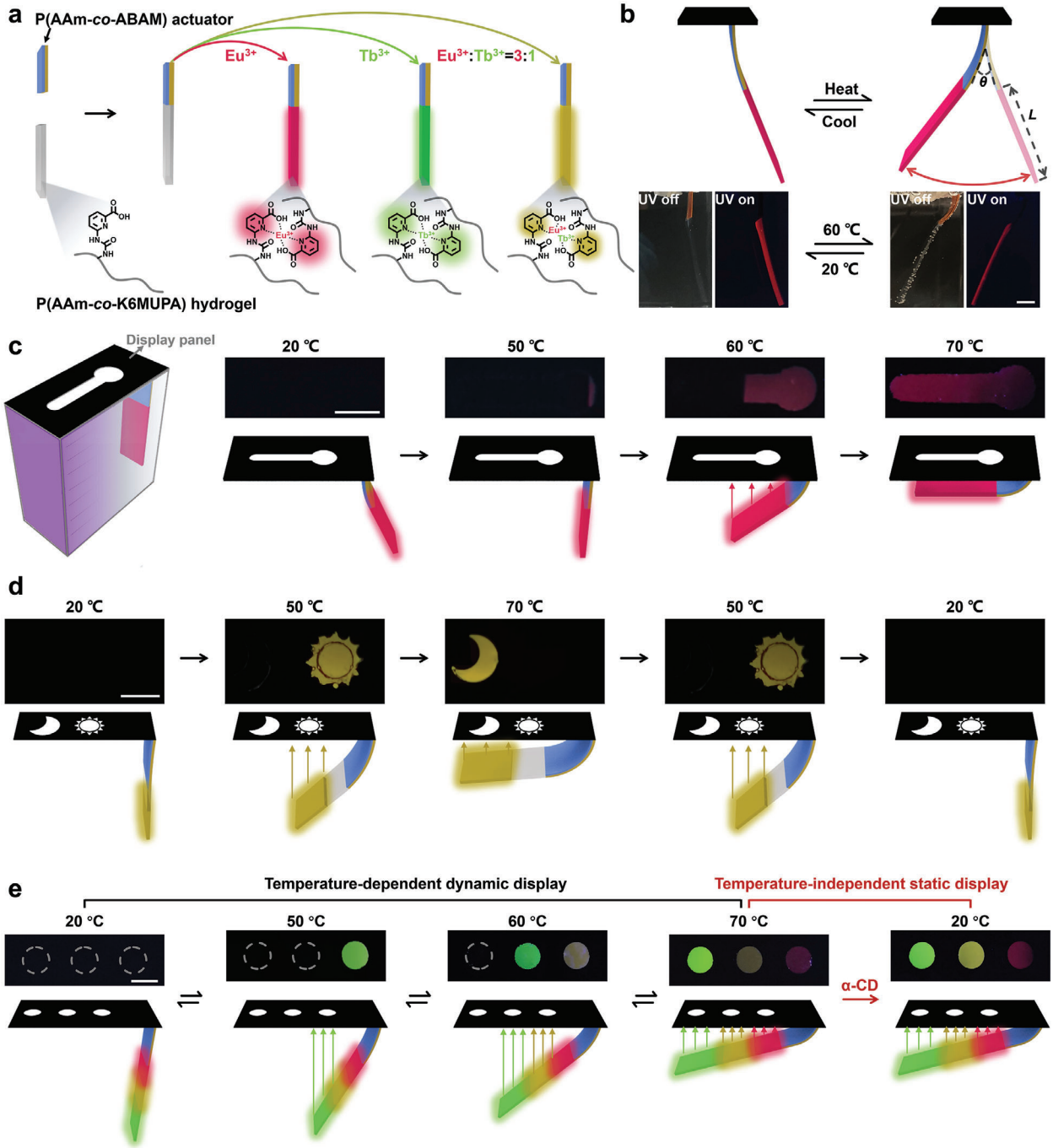

Figure 4. Thermomechanical display. a) Fabrication of multicolor fluorescent hydrogel actuators through series connection of the bilayer P(AAm-*co*-ABAM) hydrogel actuator and the Eu^{3+}/Tb^{3+}-coordinated multicolor fluorescent P(AAm-*co*-K6MUPA) hydrogel block. The emission color of fluorescent hydrogel block could be facilely adjusted to red, green, or yellow upon coordination with Eu^{3+}, Tb^{3+}, or their mixtures. b) Scheme and photo showing thermoresponsive reversible actuation process of the series-connected red fluorescent hydrogel actuator via a "thermal stimulation-hydrogel actuation-fluorescence output" cascading mechanism. Upon environment temperature elevation from 20 °C to 60 °C, it took ≈25 min to complete the shape morphing process. c) Illustration and images showing the structure of the thermomechanical display system and pattern display. For the first ≈15 min (environment temperature was 50 °C), there was no pattern displayed due to the slight deformation. Then it took ≈10 and ≈5 min, respectively, to gradually exhibit complete thermometer-like red fluorescent pattern as the environment temperature stepwisely increase to 60 °C and 70 °C. d) Illustration and images showing the temperature-dependent dynamic display results. Upon environment temperature elevation from 20 °C to 70 °C, it took ≈15 min to display "the golden sun" pattern and ≈10 min "the golden moon" pattern. Moreover, with the environment cool from 70 °C to 20 °C, "the golden moon" and "the golden sun" pattern would disappear after 15 and 30 min, respectively. e) Images showing the α-cyclodextrin (α-CD) gated intelligent switch between temperature-dependent dynamic display and temperature-independent static display via an α-CD-gated "thermal stimulation-hydrogel actuation-fluorescence output" cascading mechanism. Upon environment temperature elevation from 20 °C to 70 C, it took ≈15, ≈10, and ≈5 min, respectively, to stepwisely exhibit traffic-light like fluorescent. Scale bars: 0.5 cm.

actuator, and then reversibly recovered to bend right upon subsequent temperature decrease. As can be seen from Figure S20 (Supporting Information), such thermal actuating process was proved to be reproducible. In this way, a thermomechanically actuated system was established. Note that as long as this equilibrium deformation state was reached, this deformation state would persist. Owing to the wide UCST phase-transition window of top P(AAm-*co*-ABAM) actuator, the bending angle of bottom fluorescent hydrogel block was capable of being largely regulated by varying environmental temperature. Moreover, limited by the actuating force of top P(AAm-*co*-ABAM) actuator, the bending angle of whole system was also found to be dependent on the length of bottom fluorescent hydrogel block (Figure S21, Supporting Information). Therefore, the length of bottom fluorescent hydrogel block was optimized to be less than 40 mm in the following studies for the purpose of ensuring better display effect.

To tentatively mimic the display function of cephalopods' skin, artificial thermomechanically modulated display system was designed by tethering one end of such series-connected fluorescent hydrogel actuator onto one top suspended display panel with a hollow window. Such design was proposed to produce one promising cascading display mechanism of "thermal stimulation-hydrogel actuation-fluorescence output," which exactly resembled the natural "bioelectricity stimulation-radial muscle actuation-skin color change" display strategy of cephalopods. For the example shown in Figure 4c, no fluorescent pattern was noticed on the display panel at room temperature. Upon temperature increase to 60 °C, the tethered actuator would largely bend to partially cover the open window of top display panel, resulting in the display of red fluorescent pattern. At higher temperature (e.g., 70 °C), bending angle of the tethered actuator would be large enough to cover the whole open window, leading to the display of a complete thermometer-like red fluorescent pattern. Similarly, many other fluorescent patterns such as "the golden sun" and "the golden moon" could be dynamically and reversibly displayed in response to stepwise variation of environmental temperature (Figure 4d), when the tethered actuator was prepared by series-connecting the Eu^{3+}/Tb^{3+}-coordinated yellow light-emitting P(AAm-*co*-K6MUPA) hydrogel and bilayer P(AAm-*co*-ABAM) hydrogel actuator.

Having established the bioinspired "thermal stimulation-hydrogel actuation-fluorescence output" cascading display mechanism, we further optimized the thermomechanically modulated display system by engineering composition and structure of the series-connected fluorescent hydrogel actuators in order to achieve multifluorescence color outputs. As demonstrated in Figure 4e, three-color (red, yellow, and green) fluorescent hydrogel block was prepared and connected onto the bilayer P(AAm-*co*-ABAM) hydrogel actuator. Different-colored pattern signals would thus be displayed on the traffic-light-like display panel in response to environmental temperature change. For example, the actuator slightly bent to cover the first hole of the display panel at 50 °C, exhibiting green fluorescent signal. With continuous heating, this display system was capable of successively generating two-color fluorescent signals and three-color fluorescent signals when the environmental temperature reached 60 °C and 70 °C, respectively. Conversely, as the external environment cooled from 70 °C to room temperature, these fluorescent colors would gradually disappear because of the reversible deformability of the P(AAm-*co*-ABAM) actuator. Interestingly, if α-CD was utilized to deactivate the thermal actuating responsiveness of bilayer P(AAm-*co*-ABAM) actuator at 70 °C via supramolecular host–guest interactions, such three-color fluorescent signal would persist even when the environmental temperature was cooled to 20 °C and reheated to 70 °C, indicating the powerful capacity for temperature-independent static information display. These results demonstrated that our thermomechanically actuated display systems were capable of utilizing one single temperature stimulus to achieve dynamic multicolor outputs on the basis of temperature-dependent actuating behavior of bilayer P(AAm-*co*-ABAM) actuator. What's more, they could also be reversibly programmed to enable temperature-independent static information display by further employing the α-CD chemical to gate the thermal actuating responsiveness of bilayer P(AAm-*co*-ABAM) actuator. Such intelligent switch between dynamic and static information display modes are highly appealing to meet the differential display requirements for various kinds of information, but has previously never been achieved.

Not only the dynamic/static dual-mode display of multiple colors, cephalopods' skin also has the amazing capacity for intricate pattern display in order to deliver distinct information to the co-existing organisms. Replication of this sophisticated biological display strategy is believed to endow the information delivery function for our thermomechanically modulated display systems. To demonstrate this potential, one array-type 3D display platform was firstly demonstrated by tethering three series-connected fluorescent hydrogel actuators onto the top suspended 2D display panel. As illustrated in **Figure 5a**, actuators i and ii were identical and prepared by connecting one triple-segmented (red-none-red) fluorescent hydrogel block with the bilayer P(AAm-*co*-ABAM) actuator, while actuator iii was obtained by attaching a whole Eu^{3+}-coordinated red fluorescent hydrogel block with the bilayer P(AAm-*co*-ABAM) actuator. Based on this array-type actuating structure, dynamic multiple information output was demonstrated as follows in response to one single temperature stimulus: Initially, these three hydrogel actuators were kept upright and thus no information was observed. When the environmental temperature rose to 50 °C, bending deformation of the three actuators were triggered to expose their red fluorescent hydrogel ends, leading to the appearance of letter "I" on the display panel. With further temperature increase, these three fluorescent actuators would be largely deformed to make their central portions cover the hollow holes of display panel, resulting in self-erasure of the previous letter "I" and display of the second letter "L". Finally, when the external temperature reached 70 °C, bending angle of these hydrogel actuators would be large enough to fully cover nine holes of the display panel to show the third new letter "U". As described above, during the stepwise heating process from 20 °C to 70 °C, this information display system was capable of delivering the message "I Love U" by successively generating the letters "I," "L," and "U" in order. In this way, the desirable "single-input multiple-outputs" feature has been demonstrated for the biomimetic display system to allow on-demand delivery of multiple dynamic information by taking use of temperature-dependent synchronous actuating behaviors of several tethered hydrogel actuators.

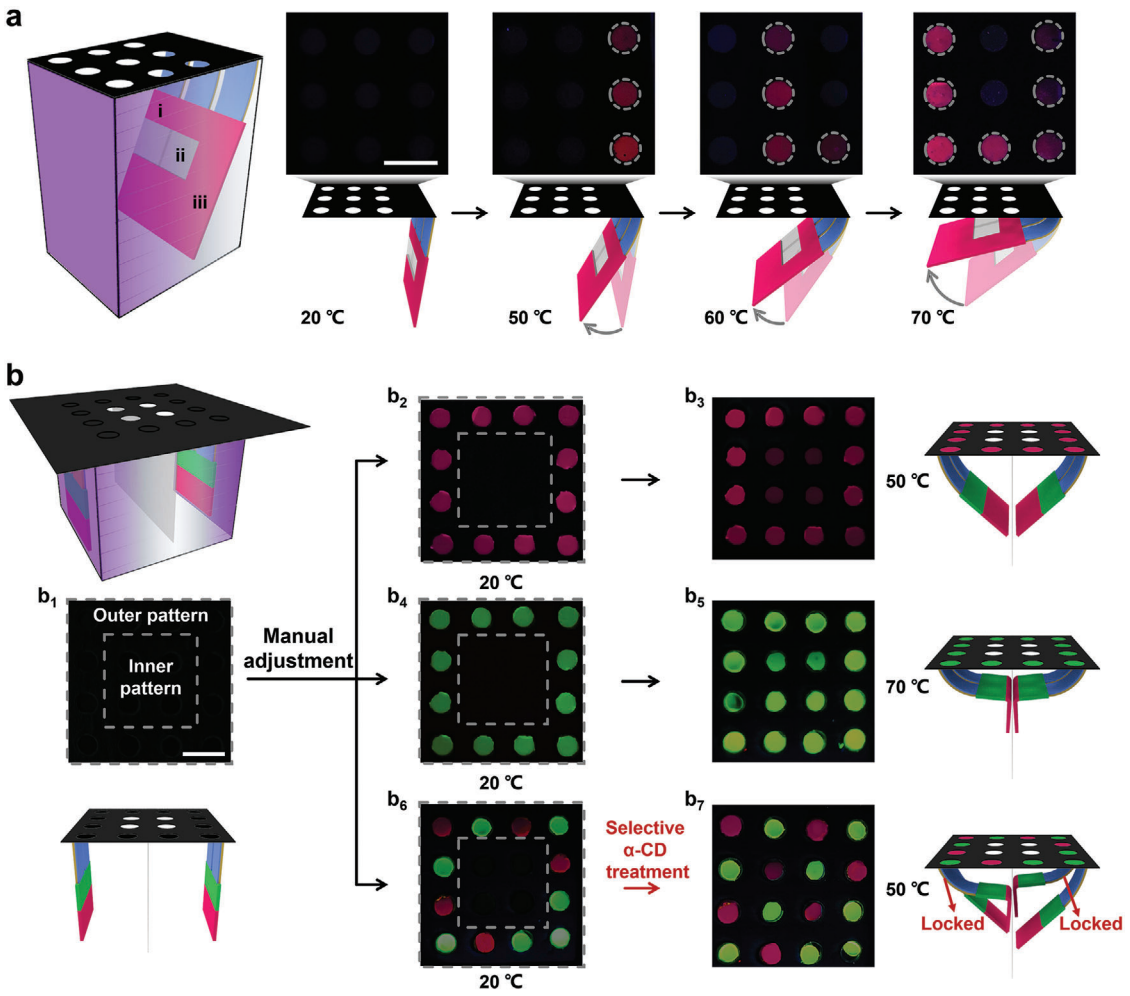

Figure 5. Array-type three-dimensional (3D) display platforms for information delivery. a) Structure of one array-type 3D display platform, as well as the illustration and images showing its temperature-dependent successive display of the letters "I," "L," and "U" in order. Upon environment temperature elevation from 20 °C to 70 °C, it took ≈15, ≈10,and ≈5 min, respectively, to display the letters "I," "L," and "U" in order. b) Structure of another array-type 3D display platform, as well as the illustration and images showing its spatially controlled display of multiple distinct information via the selective α-cyclodextrin (α-CD) gated thermomechanical responsiveness of these four tethered actuators. Upon environment temperature elevation from 20 °C to 50 °C, it took ≈15 min to display the pattern change from b_2 to b_3. Upon environment temperature elevation from 20 °C to 70 °C, it took ≈10 min to display the pattern change from b_4 to b_5. Upon environment temperature elevation from 20 °C to 50 °C, it took ≈15 min to display the pattern change from b_6 to b_7. Scale bars: 1 cm.

Another intriguing and important feature of cephalopods' skins is that they are able to intelligently secret neurotransmitter inhibitor like acetylcholine to spatially inhibit the actuating responsiveness of radial muscles around certain skin chromatophores for ensuring perfect skin color/pattern adaptation in complex natural environments. Such chemical-gated spatial control over muscle actuation further encouraged us to leverage the α-CD-gated thermomechanical responsiveness of bilayer P(AAm-*co*-ABAM) actuators to improve the information delivery results of our array-type display platform. One proof-of-concept example equipped with four identical dual-color fluorescent hydrogel actuators was illustrated in Figure 5b. To demonstrate its adaptive multipattern display capacity, fluorescent patterns on the outer part of this display panel (designed as the reference background) could be adjusted by manually placing different-colored hydrogel pieces on these outer holes (Figure 5b_1,b_2,b_4,b_6). As can be seen from Figure 5b_2,5b_3, when the environment temperature was elevated to 50 °C to bend all these four hydrogel actuators, the inner part of this display panel was capable of displaying red fluorescent pattern that matched well with that of the outer part. Similarly, when the pattern of the outer part was made to be green fluorescent, consistent fluorescent pattern could also be made to display on the inner part by merely elevating the temperature to 70 °C for triggering larger hydrogel actuation Figure 5b_4,b_5. Nevertheless, if the pattern of outer part was engineered to be multicolored (Figure 5b_6), it became impossible to allow the appearance of matched fluorescent pattern on the inner part of this display panel through simple environmental temperature variation. Fortunately, the thermoresponsiveness of two tethered hydrogel actuators could be selectively deactivated after being treated by α-CD at 70 °C. As a result, multicolored fluorescent pattern was observed on the inner

part when the temperature was cooled to 50 °C to trigger the deformation of the other two hydrogel actuators (Figure 5b$_7$). Note that the information display time after "selective α-CD treatment" was primarily influenced by the bending angle of corresponding hydrogel actuator. Therefore, the time-dependent bending angles of the hydrogel actuator were investigated in details (Figure S22, Supporting Information), which indicated that the information display time can last for about 3 h. During the actuating-display process, only a small quantity of α-CD molecules were dissociated from the α-CD-treated hydrogel actuator. Therefore, no obvious actuating performance loss were observed for the untreated hydrogel actuator. All these results demonstrated that our display system could be intelligently engineered to show spatially controlled display of multiple distinct information owing to the bioinspired α-CD-gated thermomechanical responsiveness of these four tethered actuators.

2.5. α-CD-Gated Thermomechanical Display for High-Security Information 3D-Encoding

The bioinspired thermomechanically display systems, characterized with an unprecedented combination of single-input multiple-output, dynamic/static dual-mode and spatially controlled display capacities, further enlightened us to explore their display applications for information 3D-encoding with enhanced security. To demonstrate this potential, one 3D display system was designed and illustrated in **Figure 6**a, which comprised a display panel with one predesigned QR code pattern and two hydrogel actuators with different structures. At normal conditions, no information was noticed on the display panel (Figure 6a$_1$), indicating the secure information encryption. When the temperature was raised to either 50 °C or 70 °C for triggering synchronous deformation of these two tethered actuators, the encrypted QR code could be partially observed (Figure 6a$_2$,a$_3$), but it was incomplete and thus unreadable. In other words, the true information had been safely encrypted and impossible to be decrypted by simple temperature elevation. It was only when the short hydrogel actuator was selectively treated by α-CD to lock its deforming state at 70 °C that the complete red fluorescent QR code information could be displayed at 50 °C (Figure 6a$_4$). Scanning this true QR code would successfully decrypt the encrypted information, which directed users to our group's website. In this way, the desirable information 3D-encryption display potential was demonstrated for our thermomechanically display system.

To further enhance information encryption capacity and security, two fluorescent hydrogel actuators with green and red emission colors, respectively, were integrated in the construction of thermomechanically display system. Figure 6b depicts one example, in which the display panel was designed to be potentially capable of delivering three types of information: bar code (Ningbo Institute of Material Technology and Engineering, abbreviated as "NIMTE"), QR code (Ningbo University, abbreviated as "NBU"), and one figure pattern (Logo of our group). As shown in Figure 6b$_1$, no information was displayed at room temperature. Upon environmental temperature elevation to 50 °C for synchronously bending these two tethered hydrogel actuators, only the red fluorescent pattern of our group logo could be read, because the green fluorescent bar code information was incomplete (Figure 6b$_2$). With continuous increase of environmental temperature to 70 °C, larger synchronous bending of these two tethered hydrogel actuators was caused to enable the display of all these three types of information (Figure 6b$_3$). Nevertheless, even if cyclic heating–cooling process was applied (Figure S23, Supporting Information), these displayed information were still confusing, because it was still unclear whether our group belonged to Ningbo Institute of Material Technology and Engineering (NIMTE) or Ningbo University (NBU). Therefore, the correct information could only be deciphered by the designated inspectors who selectively treated the green fluorescent hydrogel actuator in α-CD solution at 70 °C for erasing its thermoresponsiveness and then decreased the environment temperature to 50 °C (Figure 6b$_4$). Note that such sequential "α-CD treatment and temperature decrease" key to the true information was usually unknown to the public, suggesting its quite good information encryption application potential.

3. Conclusion

In summary, by replicating the chemical-gated actuation control function of Cephalopods' skin muscles for on-demand color/pattern display, a supramolecular host–guest interaction gating strategy was proposed to dynamically program and gate the thermoresponsiveness of smart hydrogel actuators after material manufacture, followed by the demonstration of robust chemical-gated 3D-encoding information carriers with enhanced display security. The material design relied on the hydrophobic azobenzene-functionalized PAAm hydrogels, whose UCST-type responsiveness could be gated by the addition of hydrophilic α-CD molecules to bind the grafted azobenzene moieties via host–guest interactions. On this basis, bioinspired α-CD-gated multicolor fluorescent hydrogel actuators were constructed, which could be capable of acting as analogues of Cephalopods' skin muscles to enable the development of new-concept 3D display systems. On the basis of these characteristics, high-security information 3D-encoding carriers were constructed to enable chemical-gated multiple information display.

To endow artificial soft hydrogel actuators with life-like chemical-gated control function, and then make most of their α-CD-gated actuation behaviors to develop robust multifunction-integrated display systems for high-security information 3D-encoding is the key point of our present work. Compared with most of traditional information 2D-encoding carriers relying on stimuli-responsive chemical actions for reversible data encoding/decoding, the proposed 3D-encoding strategy has been demonstrated to actually one thermomechanical display process via a conceptually new α-CD-gated "thermal stimulation-hydrogel actuation-fluorescence output" cascading mechanism. As detailed in this study, such α-CD-gated 3D-encoding systems brought many promising advantages, including single-input multiple-output, dynamic/static dual-mode, and spatially controlled display capacities. These desirable multifunction-integrated merits are highly appealing but have never been combined previously in one single luminescent display system. Moreover, the proposed strategy to construct chemical-gated artificial soft actuators is believed to be generally applicable. Besides the host–guest interactions studied herein, many other supramolecular or dynamic covalent interactions are also expected to be

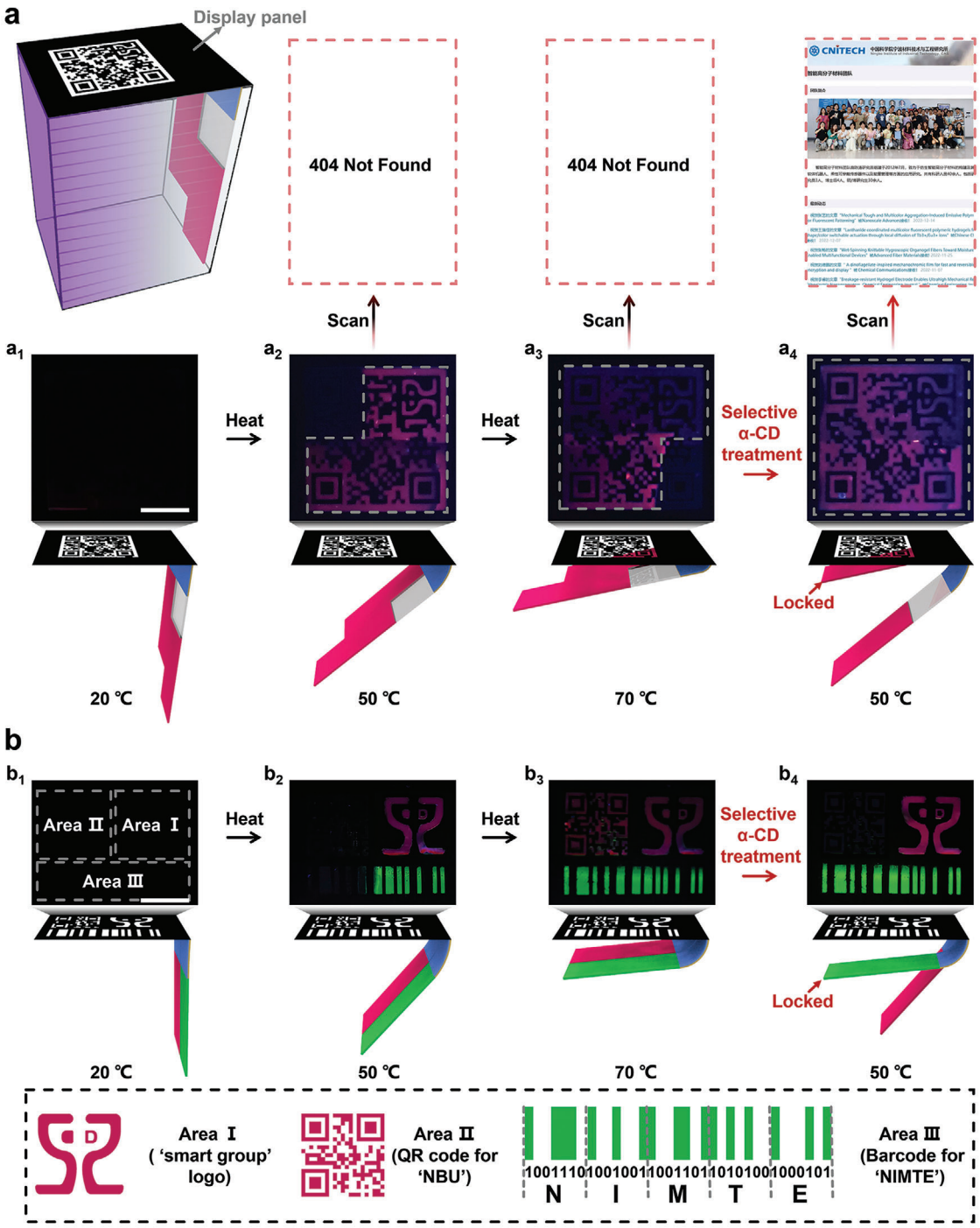

Figure 6. α-cyclodextrin (α-CD) gated thermomechanical display for information three-dimensional (3D) encoding. a) Structure of the 3D-encoding information carrier, as well as the illustration and image showing its temperature-dependent stepwise information display and α-CD-gated correct information decryption. Upon environment temperature elevation from 20 °C to 70 °C, it took ≈15 and ≈10 min, respectively, to display the pattern of a_2 and a_3 in order. After selectively treated by α-CD, it took ≈30 min to display the complete QR code. b) Illustration and images showing its temperature-dependent stepwise (logo pattern, QR code and barcode) information display, as well as the α-CD-gated correct information decryption. Upon environment temperature elevation from 20 °C to 70 °C, it took ≈15 and ≈10 min, respectively, to display the pattern of b_2 and b_3 in order. After selectively treated by α-CD, it took ≈20 min to display the complete QR code. Scale bars: 1 cm.

employed to achieve the life-like chemical-gated control function in artificial systems. We hope the success of this work will be a starting point to inspire better actuating materials and luminescent display systems for future research.

4. Experimental Section

Materials: Acrylamide (AAm), dichloromethane (DCM), sodium hydroxide (NaOH), hydrochloric acid (HCl) were purchased from Sinopharm Chemical Reagent Co. Ltd. Triethylamine, urea, *N*,*N*'-methylenebisacrylamide (BIS), ammonium persulfate (APS), tetramethylethylenediamine (TEMED), hexylamine, α-cyclodextrin, sodium alginate (Alg), calcium chloride ($CaCl_2$), 6-amino-2-pyridinecarboxylic acid, ethyl isocyanate methacrylate, terbium nitrate ($Tb(NO_3)_3{\cdot}5H_2O$), europium nitrate ($Eu(NO_3)_3{\cdot}6H_2O$) were purchased from Aladdin reagent Co. Ltd. Tetrahydrofuran (THF) was purchased from J&K Scientific reagent Co. Ltd. Aminoazobenzene was purchased from Macklin reagent Co. Ltd. All the chemicals were used as received.

Instruments and Characterization: The lyophilizing process was conducted in the DGJ-10C freeze dryer (Shanghai Boden Biological Science and Technology Co. Ltd.). The transmittance was characterized using UV–Vis Spectrophotometer (USB2000+XR1-ES) with the heating and cooling rate of 1 °C min^{-1}. Dynamic rheological measurements of hydrogels with 25 mm parallel plates were conducted with rheometer (HR-3, TA) on a temperature sweep (3 °C min^{-1}) at a constant angular frequency of 10 rad s^{-1} and shear strain of 2%. The hydrogel hydrophobicity was evaluated by dynamic contact angle measuring instrument (OCA25). The chemical environment of hydrogel was evaluated by confocal micro Raman spectroscopy (Renishaw in Via-Reflex) and micro infrared spectroscopy (Cary660+620) in corresponding temperature. The patterned hydrogels were obtained by laser cutter (GY-460 bought from Shandong Liaocheng Guangyue laser equipment Co. Ltd.) with 20% output power. All simulations were carried out using Abaqus 2020. The Abaqus/Standard solver was employed. The models of the actuators were constructed using 4-node doubly curved thin or thick shell, reduced integration, hourglass control, and finite membrane strains elements (S4R). The mechanical property of the hydrogels was captured using linear elastic model with uniaxial tension test data, and the swelling behavior of hydrogel was captured using isotropic expansion from swelling test data. Images taken by mobile phones were processed by edge extraction, brightness, and contrast in the article.

Synthesis of Azo-Acrylamide (ABAM) Monomer: The ABAM monomer was synthesized from the reaction between aminoazobenzene and acryloyl chloride via a reported method. In detail, aminoazobenzene (5 g, 20 mmol), triethylamine (4 mL, 28 mmol) was added into ultradry THF (180 mL) in a 500 mL flask and keep in ice water bath. After sufficient stirring, acryloyl chloride (2.3 mL, 28 mmol) was dropwise to the above solution. After reacting at room temperature for 3.5 h, filtered the product and removed excess THF via rotary evaporator. Then, the product was recrystallized by 80 mL DCM. Finally, filtered the product and dried it in vacuum oven. The productivity was about 50%.

Fabrication of P(AAm-co-ABAM) Hydrogel: AAm (710 mg), ABAM (126 mg), BIS (65 mg), APS (56 mg), TEMED (10 µL), and DMSO (5 mL) were mixed to form an aqueous solution. Then the hydrogel precursor was added into a 1 mm thick mold. The polymerization was carried out at 70 °C for 12 h. After polymerization, the P(AAm-co-ABAM) hydrogel was immersed in deionized water to exchange the DMSO and remove unreacted monomer.

Preparation of Bilayer Hydrogel Actuator: The P(AAm-*co*-ABAM) hydrogel was firstly immersed into 15 mg mL^{-1} APS solution. After 5 min, took out the hydrogel and wiped dry the surface. Then, the hydrogel precursor (composed of 0.2 g alginate, 710 mg AAm, 21.3 mg BIS, 150 µL TEMED and 10 mL deionized water) was poured onto the surface of P(AAm-*co*-ABAM) hydrogel. After 10 min, the bilayer hydrogel was obtained after washing the ungelatinized precursor by deionized water and treated with appropriate 0.1 M $CaCl_2$ to enhance the mechanical property.

Synthesis of 6-(3-(2-(Methacryloyloxy) Ethyl) Ureido) Picolinic Acid (K6MUPA) Fluorescent Monomer: The K6MUPA fluorescent monomer was synthesized from the reaction between aminoazobenzene and acryloyl chloride via a reported method.[18] In detail, 6-amino-pyridine-2-carboxylic acid (3.45 g, 24.98 mmol) and triethylamine (7 mL) were added into 125 mL dry DCM. Then, a mixture solution contained of DCM (50 mL) and 2-isocyanatoethylmethacrylate (5.30 mL, 37.51 mmol) was dropwise into the above solution in ice water bath. After kept this reaction for 96 h at room temperature. The excess solvent was removed by rotary evaporation and poured the product into 500 mL pouring deionized water. Subsequently, the product would be precipitated from the water after slowly adjusting the pH value to 2 by 1 M HCl solution. Finally, filtered the product and dried it in vacuum oven. The productivity was about 30%.

Fabrication of P(AAm-co-K6MUPA) Hydrogel: AAm (710 mg), K6MUPA (60 mg), NaOH (20 mg), BIS (21.3 mg), APS (21.3 mg), TEMED (10 µL), and deionized water (10 mL) were mixed to form an aqueous solution. Then the hydrogel precursor was added into a 1 mm thick mold. The polymerization was carried out at room temperature for 12 h. After polymerization, the P(AAm-*co*-K6MUPA) hydrogel was immersed in deionized water to remove unreacted monomer and reached a swelling equilibrium. It is worth noting that immersing the P(AAm-*co*-K6MUPA) hydrogel into Eu^{3+} and Te^{3+} could obtain corresponding red and green fluorescent hydrogel, respectively.

Selective α-CD Treatment: The chosen hydrogel actuator was dismantled from the display system and then immersed into the α-CD solution (5 mg L^{-1}) to diminish its UCST-type responsiveness. Then, such α-CD-treated hydrogel actuator was installed into the display system to achieve spatially controlled display of multiple distinct information.

Statistical Analysis: The value of relative transmission was normalized to the value of transmission in 80 °C. All experiments were repeated at least three times. The error bars of experimental data were repeated at least four times and presented with mean ± standard deviation (SD). The size of samples for the swelling ratio measure were 25 × 3 × 0.6 mm. The size of samples for the Raman, transmittance, FT-IR, and contact angle were 20 × 20 × 0.6 mm. The hydrogel actuator appeared in Figure 3, Figures S17–S19 (Supporting Information) were 25 × 3 × 1 mm. The bilayer hydrogel actuators appeared in Figures 4–6 were 20 × 10 × 1 mm. The software of Excel was employed to conduct one-way analysis of variance (one-way ANOVA) and the difference among samples was considered to be important when the calculated *p*-value was lower than 0.05.

Supporting Information

Supporting Information is available from the Wiley Online Library or from the author.

Acknowledgements

B.Y.W. and M.Q.S. contributed equally to this work. The authors thank the constructive discussion with Prof. Partick Théato in Karlsruhe Institute of Technology (Germany). This work was supported by Natural Science Foundation of China (22322508), the National Key Research and Development Program of China (2022YFB3204300), Zhejiang Provincial Natural Science Foundation of China (LD22E050008), International Cooperation Project of Ningbo City (2023H019), and the Sino-German mobility program (M-0424).

Conflict of Interest

The authors declare no conflict of interest.

Data Availability Statement

The data that support the findings of this study are available from the corresponding author upon reasonable request.

Keywords

bioinspired materials, chemical-gated actuation, fluorescent patterning, hydrogel, information 3D-encoding

Received: January 31, 2024
Revised: March 14, 2024
Published online:

[1] a) D. J. Jiao, Q. L. Zhu, C. Y. Li, Q. Zheng, Z. L. Wu, *Acc. Chem. Res.* **2022**, *55*, 1533; b) B. Y. Wu, H. H. Lu, X. X. Le, W. Lu, J. W. Zhang, P. Théato, T. Chen, *Chem. Sci.* **2021**, *12*, 6472; c) G. Isapour, M. Lattuada, *Adv. Mater.* **2018**, *30*, 1707069; d) L. Montero de Espinosa, W. Meesorn, D. Moatsou, C. Weder, *Chem. Rev.* **2017**, *117*, 12851.

[2] a) W. Lu, M. Q. Si, X. X. Le, T. Chen, *Acc. Chem. Res.* **2022**, *55*, 2291; b) B. Y. Wu, H. H. Lu, Y. K. Jian, D. C. Zhang, Y. Peng, J. Zhuo, X. X. Le, J. W. Zhang, P. Théato, T. Chen, *CCS Chem.* **2022**, *5*, 704; c) X. F. Ji, Z. Li, Y. B. Hu, H. L. Xie, W. J. Wu, F. Y. Song, H. X. Liu, J. G. Wang, M. J. Jiang, J. W. Y. Lam, B. Z. Tang, *CCS Chem.* **2021**, *3*, 1146; d) H. Hu, C. Huang, M. Galluzzi, Q. Ye, R. Xiao, X. F. Yu, X. M. Du, *Research* **2021**, *2021*, 9786128.

[3] a) Q. M. Wang, G. R. Gossweiler, S. L. Craig, X. H. Zhao, *Nat. Commun.* **2014**, *5*, 4899; b) Y. P. Wang, X. F. Cao, J. Cheng, B. W. Yao, Y. S. Zhao, S. L. Wu, B. Z. Ju, S. F. Zhang, X. M. He, W. B. Niu, *ACS Nano* **2021**, *15*, 3509; c) D. Han, Y. P. Wang, C. Yang, H. Lee, *ACS Appl. Mater. Interfaces* **2021**, *13*, 12735.

[4] a) J. B. Messenger, *Biol. Rev. Cambridge Philos. Soc.* **2001**, *76*, 473; b) S. X. Wei, W. Lu, H. H. Shi, S. S. Wu, X. X. Le, G. Q. Yin, Q. Q. Liu, T. Chen, *Adv. Mater.* **2023**, *35*, 2300615; c) H. H. Shi, S. S. Wu, M. Q. Si, S. X. Wei, G. Q. Lin, H. Liu, W. P. Xie, W. Lu, W. Chen, *Adv. Mater.* **2022**, *34*, 2107452.

[5] J. B. Messenger, *Invertebr. Neurosci.* **1996**, *2*, 95.

[6] a) S. Wei, W. Lu, H. Shi, S. Wu, X. Le, G. Yin, Q. Liu, T. Chen, *Adv. Mater.* **2023**, *35*, 2300615; b) J. Bai, Z. X. Shi, X. S. Jiang, *Adv. Funct. Mater.* **2023**, *33*, 2301797; c) C. C. Li, J. Z. Liu, X. Y. Qiu, X. Yang, X. Huang, X. X. Zhang, *Angew. Chem., Int. Ed.* **2023**, *62*, e202313971.

[7] a) D. Y. Lou, Y. J. Sun, J. Li, Y. Y. Zheng, Z. P. Zhou, J. Yang, C. X. Pan, Z. K. Zheng, X. O. Chen, W. Liu, *Angew. Chem., Int. Ed.* **2022**, *61*, 202117066; b) Y. Sun, X. X. Le, S. Y. Zhou, T. Chen, *Adv. Mater.* **2022**, *34*, 2201262; c) K. Lou, Z. Q. Hu, H. W. Zhang, Q. Y. Li, X. F. Ji, *Adv. Funct. Mater.* **2022**, *32*, 2113274; d) Y. B. Yang, Q. Y. Li, H. W. Zhang, H. Liu, X. F. Ji, B. Z. Tang, *Adv. Mater.* **2021**, *33*, 2105418; e) S. X. Wei, Z. Li, W. Lu, H. Liu, J. W. Zhang, T. Chen, B. Z. Tang, *Angew. Chem., Int. Ed.* **2020**, *59*, 2; f) Y. Shen, X. X. Le, Y. Wu, T. Chen, *Chem. Soc. Rev.* **2024**, *53*, 606.

[8] a) J. J. Gao, M. Tian, Y. R. He, H. J. Yi, J. B. Guo, *Adv. Funct. Mater.* **2021**, *32*, 2107145; b) H. W. Zhang, Q. Y. Li, Y. B. Yang, X. F. Ji, J. L. Sessler, *J. Am. Chem. Soc.* **2021**, *143*, 18635; c) Q. Wang, Z. Qi, Q. M. Wang, M. Chen, B. Y. Lin, D. H. Qu, *Adv. Funct. Mater.* **2022**, *32*, 2208865; d) D. L. Wang, J. Y. Gong, Y. Xiong, H. Z. Wu, Z. Zhao, D. Wang, B. Z. Tang, *Adv. Funct. Mater.* **2022**, *33*, 2208895.

[9] a) Y. C. Zhang, X. X. Le, Y. K. Jian, W. Lu, J. W. Zhang, T. Chen, *Adv. Funct. Mater.* **2019**, *29*, 1905514; b) J. Y. Zhang, H. C. Shen, X. Y. Liu, X. Q. Yang, S. L. Broman, H. R. Wang, Q. Y. Li, J. W. Y. Lam, H. K. Zhang, M. Cacciarini, M. B. Nielsen, B. Z. Tang, *Angew. Chem., Int. Ed.* **2022**, *61*, e2022084; c) J. Guo, S. S. Wu, Y. L. Wang, J. H. Huang, H. Xie, S. B. Zhou, *Mater. Horiz.* **2022**, *9*, 3039; d) Z. Q. Li, G. N. Wang, Y. X. Ye, B. Li, H. R. Li, B. L. Chen, *Angew. Chem., Int. Ed.* **2019**, *58*, 18025; e) H. Q. Ju, H. K. Zhang, L. X. Hou, M. Zuo, M. Du, F. Huang, Q. Zheng, Z. L. Wu, *J. Am. Chem. Soc.* **2023**, *145*, 3763.

[10] a) X. X. Le, H. Shang, H. Z. Yan, J. W. Zhang, W. Lu, M. J. Liu, L. P. Wang, G. M. Lu, Q. J. Xue, T. Chen, *Angew. Chem., Int. Ed.* **2020**, *59*, 2; b) X. F. Ji, Z. Li, X. L. Liu, H. Q. Peng, F. Y. Song, J. Qi, J. W. Y. Lam, L. L. Long, J. L. Sessler, B. Z. Tang, *Adv. Mater.* **2019**, *31*, 1902365; c) J. H. Huang, Y. Jiang, Q. Y. Chen, H. Xie, S. B. Zhou, *Nat. Commun.* **2023**, *14*, 7131; d) Z. H. Wang, Y. Zheng, Y. Su, L. Gao, Y. Y. Zhu, J. Xia, Y. F. Zhang, C. Wang, X. Zheng, Y. L. Zhao, C. L. Yang, Y. B. Li, *Sci. China Mater.* **2021**, *65*, 2160.

[11] a) B. Ma, C. T. Xu, L. S. Cui, C. Zhao, H. Liu, *ACS Appl. Mater. Interfaces* **2021**, *13*, 5574; b) D. Chen, C. Ni, C. Yang, Y. Li, X. Wen, C. W. Frank, T. Xie, H. Ren, Q. Zhao, *Adv. Mater.* **2023**, *35*, 2209956; c) Y. X. Shang, Z. Y. Chen, F. F. Fu, L. Y. Sun, C. M. Shao, W. Jin, H. Liu, Y. J. Zhao, *ACS Nano* **2018**, *13*, 796; d) C. N. Zhu, T. W. Bai, H. Wang, J. Ling, F. H. Huang, W. Hong, Q. Zheng, Z. L. Wu, *Adv. Mater.* **2021**, *33*, 2102023; e) C. T. Yu, H. L. Guo, K. Cui, X. Y. Li, Y. N. Ye, T. Kurokawa, J. P. Gong, *Proc. Natl. Acad. Sci. U. S. A.* **2020**, *117*, 18962; f) Z. Q. Li, H. Z. Chen, B. Li, Y. M. Xie, X. L. Gong, X. Liu, H. R. Li, Y. L. Zhao, *Adv. Sci.* **2019**, *6*, 1901529; g) W. Zhang, B. H. Wu, S. T. Sun, P. Y. Wu, *Nat. Commun.* **2021**, *12*, 4082; h) Q. L. Zhu, C. Du, Y. H. Dai, M. Daab, M. Matejdes, J. Breu, W. Hong, Q. Zheng, Z. L. Wu, *Nat. Commun.* **2020**, *11*, 5166; i) F. F. Fu, L. R. Shang, Z. Y. Chen, Y. R. Yu, Y. J. Zhao, *Sci. Rob.* **2018**, *3*, eaar8580; j) S. Y. Zhuo, Z. G. Zhao, Z. X. Xie, Y. F. Hao, Y. C. Xu, T. Y. Zhao, H. J. Li, E. M. Knubben, L. Wen, L. Jiang, M. J. Liu, *Sci. Adv.* **2020**, *6*, eaax1464; k) H. Yuk, C. E. Varela, C. S. Nabzdyk, X. Y. Mao, R. F. Padera, E. T. Roche, X. H. Zhao, *Nature* **2019**, *575*, 169; l) Q. Li, Y. W. Zhang, C. F. Wang, D. A. Weitz, S. Chen, *Adv. Mater.* **2018**, *30*, 1803475; m) B. Li, Z. H. Song, K. Y. Zhu, Q. Y. Niu, Z. Q. Li, H. R. Li, *ACS Appl. Mater. Interfaces* **2021**, *13*, 20633; n) Y. Zhang, K. K. Liu, T. Liu, C. J. Ni, D. Chen, J. M. Guo, C. Liu, J. Zhou, Z. Jia, Q. Zhao, P. J. Pan, T. Xie, *Nat. Commun.* **2021**, *12*, 6155; o) C. J. Ni, D. Chen, Y. Yin, X. Wen, X. L. Chen, C. Yang, G. C. Chen, Z. Sun, J. H. Wen, Y. R. Jiao, C. Y. Wang, N. Wang, X. X. Kong, S. H. Deng, Y. Q. Shen, R. Xiao, X. M. Jin, J. Li, X. Q. Kong, Q. Zhao, T. Xie, *Nature* **2023**, *622*, 748; p) Z. Li, P. C. Liu, X. F. Ji, J. Y. Gong, Y. B. Hu, W. J. Wu, X. N. Wang, H. Q. Peng, R. T. K. Kwok, J. W. Y. Lam, J. Lu, B. Z. Tang, *Adv. Mater.* **2020**, *32*, 1906493.

[12] C. Z. Zhao, Z. Y. Ma, X. X. Zhu, *Prog. Polym. Sci.* **2019**, *90*, 269.

[13] J. H. Yoon, S. Yoon, *Phys. Chem. Chem. Phys.* **2011**, *13*, 12900.

[14] G. Xu, J. X. Zhang, R. T. Jia, W. Li, A. F. Zhang, *Macromolecules* **2022**, *55*, 630.

[15] C. Z. Zhao, J. L. Lu, X. X. Zhu, *ACS Appl. Polym. Mater.* **2019**, *2*, 256.

[16] a) Y. X. Cao, L. X. Ren, Y. W. Zhang, X. T. Lu, X. C. Zhang, J. T. Yan, W. Li, T. Masuda, A. F. Zhang, *Macromolecules* **2021**, *54*, 7621; b) Z. Y. Lei, P. Y. Wu, *ACS Nano* **2018**, *12*, 12860.

[17] G. Beaudoin, A. Lasri, C. Z. Zhao, B. Liberelle, G. De Crescenzo, X. X. Zhu, *Macromolecules* **2021**, *54*, 7963.

[18] W. N. Li, H. Zhang, W. Lu, Y. Zhang, T. J. Zheng, G. L. Yang, T. Chen, *Adv. Opt. Mater.* **2023**, *11*, 2202738.